Automatic Brain Tumor Segmentation by Subject Specific Modification of Atlas Priors[1]

Marcel Prastawa, BS, Elizabeth Bullitt, MD, Nathan Moon, MS, Koen Van Leemput, PhD, Guido Gerig, PhD

Rationale and Objectives. Manual segmentation of brain tumors from magnetic resonance images is a challenging and time-consuming task. An automated system has been developed for brain tumor segmentation that will provide objective, reproducible segmentations that are close to the manual results. Additionally, the method segments white matter, grey matter, cerebrospinal fluid, and edema. The segmentation of pathology and healthy structures is crucial for surgical planning and intervention.

Materials and Methods. The method performs the segmentation of a registered set of magnetic resonance images using an expectation-maximization scheme. The segmentation is guided by a spatial probabilistic atlas that contains expert prior knowledge about brain structures. This atlas is modified with the subject-specific brain tumor prior that is computed based on contrast enhancement.

Results. Five cases with different types of tumors are selected for evaluation. The results obtained from the automatic segmentation program are compared with results from manual and semi-automated methods. The automated method yields results that have surface distances at roughly 1–4 mm compared with the manual results.

Conclusion. The automated method can be applied to different types of tumors. Although its performance is below that of the semi-automated method, it has the advantage of requiring no user supervision.

Key Words. Brain tumor segmentation; expectation-maximization; level-set evolution; spatial atlas.

The task of manually segmenting brain tumors from magnetic resonance imaging (MRI) is generally time-consuming and difficult. In most settings, the task is performed by marking the tumor regions slice-by-slice, which limits the human rater's view and generates jaggy images as in Figure 1. Manual segmentation is also typically performed largely based on a single image with intensity enhancement provided by an injected contrast agent. As a result, the segmented images are less than optimal. An automatic or semi-automatic segmentation method is desirable because it reduces the load on the human raters and generates segmentations that take the information within the entire 3-dimensional (3D) multiparameter images into account.

The process of automatically segmenting medical images, as opposed to natural scenes, has the significant advantage that structural and intensity characteristics are well-known up to a natural biological variability or the presence of pathology. The most common class of methods is pixel- or voxel-based statistical classification using multiparameter images (1,2). These methods do not consider global shape and boundary information. Applied to brain tumor segmentation, classification approaches have met with only limited success (3,4) because of overlapping intensity distributions of healthy tissue, tumor, and surrounding edema. Often, lesions

Acad Radiol 2003; 10:1341–1348

[1] From the Departments of Computer Science, CB #3175, Sitterson Hall, Chapel Hill, NC 27599 (M.P., N.M., G.G.), Surgery (E.B.), and Psychiatry (G.G.), University of North Carolina, Chapel Hill, NC; and the Department of Radiology (K.L.), Helsinki University Central Hospital, Helsinki, Finland. Received May 20, 2003; revision requested August 4; received in revised form August 18, 2003; accepted August 20, 2003. Supported by NIH-NCI R01 CA67812 and NIH-NIBIB R01 EB000219 (current): 3D Cerebral Vessel Location for Surgical Planning. **Address correspondence to** M.P.

doi:10.1016/S1076-6332(03)00506-3

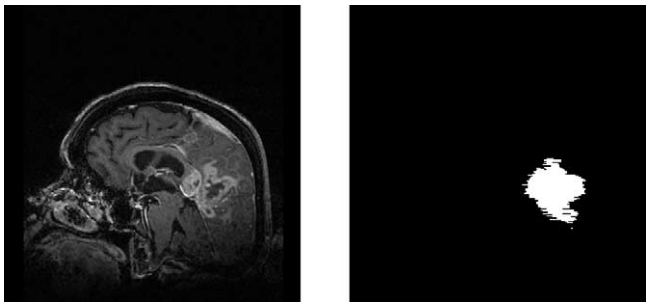

Figure 1. Gadolinium contrast enhanced T1-weighted MR image (sagittal view) and the manual tumor segmentation result. Note the "striping" effect caused by segmenting the tumor slice-by-slice in axial direction (Tumor031 data).

or tumors were considered as outliers of a mixture Gaussian model for the global intensity distribution (5,6), assuming that lesion voxels are distinctly different from normal tissue characteristics. Other approaches involve interactive segmentation tools (7), mathematical morphology (8), or calculation of texture differences between normal and pathological tissue (9).

A geometric prior can be used by atlas-based segmentation, which regards segmentation as a registration problem in which a fully labeled, template MR volume is registered to an unknown dataset. High-dimension warping results in a one-to-one correspondence between the template and subject images, resulting in a new, automatic segmentation. These methods require elastic registration of images to account for geometric distortions produced by pathologic processes. Such registration remains challenging and is not yet solved for the general case.

Warfield et al (10,11) combined elastic atlas registration with statistical classification. Elastic registration of a brain atlas helped to mask the brain from surrounding structures. A further step uses "distance from brain boundary" as an additional feature to improve separation of clusters in multidimensional feature space. Initialization of probability density functions still requires a supervised selection of training regions. The core idea, namely to augment statistical classification with spatial information to account for the overlap of distributions in intensity feature space, is part of the new method presented in this article.

Wells et al (12) introduced expectation maximization (EM) as an iterative method that interleaves classification with bias field correction. Van Leemput et al (13,14) extended the concept and developed automatic segmentation of MRI of normal brains by statistical classification, using an atlas prior for initialization and also for geometric constraints. A most recent extension detects brain lesions as outliers (15) and was successfully applied for detection of multiple sclerosis lesions. Brain tumors, however, cannot be simply modeled as intensity outliers because of overlapping intensities with normal tissue and/or significant size.

We propose a fully automatic method for segmenting MR images presenting tumor and edema, both mass-effect and infiltrating structures. This method builds on the previously published work by Van Leemput, et al (13,14). Additionally, tumor and edema classes are added to the segmentation as was done by Moon et al (16). The spatial atlas used as a prior in the classification is modified to include prior probabilities for tumor and edema. Our method provides a full classification of brain tissue into white matter, grey matter, cerebrospinal fluid (CSF), tumor, and edema. Because the method is fully automatic, its results are fully reproducible in repeated trials.

MATERIALS AND METHODS

Tumor Characteristics and Assumptions

Brain tumors are difficult to segment because they have a wide range of appearance and effect on surrounding structures. Following are some of the general characteristics of brain tumors: (A) vary greatly in size and position, (B) vary greatly in the way they show up in MRI, (C) may have overlapping intensities with normal tissue, (D) may be space occupying (new tissue that moves normal structure) or infiltrating (changing properties of existing tissue), (E) may enhance fully, partially, or not at all, with contrast agent, and (F) may be accompanied by surrounding edema (swelling).

To make the problem more tractable, we made some simplifying assumptions and focus only on a subset of tumor types. Tumors are assumed to be ring enhancing or fully enhancing with contrast agent. Furthermore, we assume that the tumor does not cause large deformation of normal brain tissues. These deformations should be small enough that they are embodied in the probabilistic brain atlas. The method requires that both enhancing and nonenhancing parts of the tumor have similar appearance characteristics when contrast is not used. The major tumor classes that fall in this category, and hence are the tumor types that we have focused on, are meningiomas and malignant gliomas. The basic characteristics of meningiomas are smooth boundaries, normally space occupying, and smoothly and fully enhancing with contrast agent. The basic characteristics of malignant gliomas are (A) ragged boundaries, (B) initially only in white matter, possibly later spreading outside white matter, (C) margins

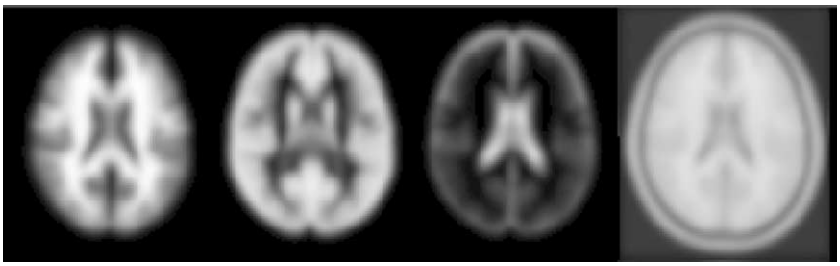

Figure 2. The ICBM digital brain atlas. From left to right: white matter probabilities, grey matter probabilities, CSF probabilities, and the T1 template.

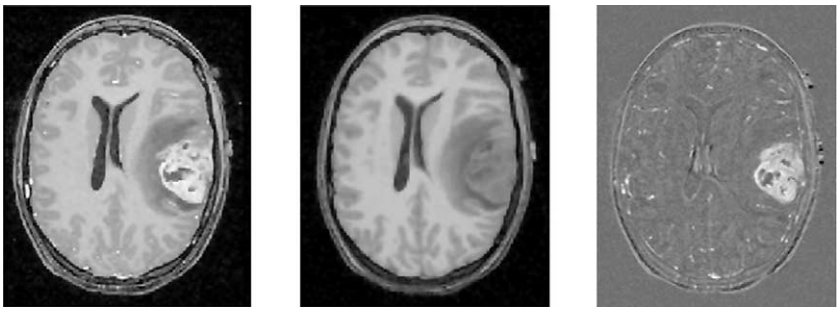

Figure 3. Computation of the difference image from registered T1 postcontrast and precontrast images. From left to right: T1 postcontrast, T1 precontrast, and the difference image with tumor that appears bright (Tumor020 data).

enhance with contrast agent, inside does not, (D) accompanied by edema, and (E) infiltrating at first, possibly becoming space occupying when larger. We also assume that all the datasets contain a T1 precontrast image, a T1 postcontrast image, and a T2 image.

Spatial Atlas

The segmentation algorithm uses a spatial probabilistic brain atlas (17) as shown in Figure 2. The brain atlas was created by averaging manual segmentations of normal brains that have been registered using affine transformation. The atlas performs two critical functions: it provides spatial prior probabilities and it is used to estimate the initial intensity distribution parameters for the normal tissue classes. For each dataset, the three different image channels are first registered to a common space and then registered to the brain atlas. The registration process is performed using affine transformation and the mutual information metric (18). Because the atlas is a normal brain atlas, it does not contain the prior probabilities for the tumor and edema. It is necessary to obtain prior probabilities for tumor and edema. Otherwise, the voxels would be incorrectly classified as normal tissue. The problem is tackled by artificially generating prior probabilities for tumor and edema.

The tumor prior probability image is generated from the difference of the T1 postcontrast and the T1 precontrast images $I_{diff} = I_{T1post} - I_{T1pre}$. This difference image (Fig 3) is then converted to probability values through histogram analysis. The histogram shows a peak around zero, with a positive response corresponding to contrast enhancement. We model the histogram using two Gaussian distributions corresponding to noise and a gamma distribution for the contrast enhancement (Fig 4). The noise in the image is represented with two Gaussian distributions based on the analysis of the difference image histogram of the datasets we have available. We have observed that the noise component can be well represented by a Gaussian with a large width and another one with a small width. The means of the two Gaussian distributions and the location parameter of the gamma distribution are constrained to be equal. From the model, we then compute a mapping that converts the difference image into a probabilistic measure of enhancement. The posterior probability of the gamma distribution is used as the map function (Fig 5), which is essentially a soft threshold on the difference image. It is important to note that after the T1 postcontrast image is used with the precontrast image to generate the tumor prior it is no longer used in

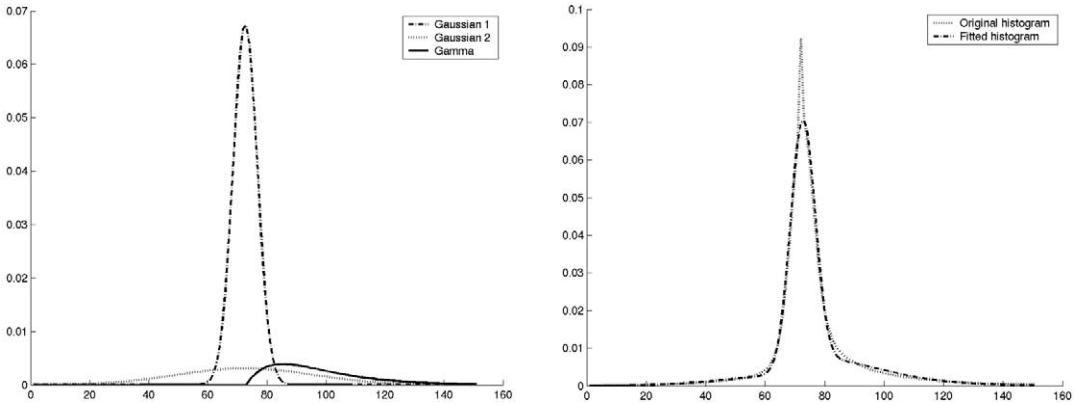

Figure 4. **(Left)** The T1 postcontrast and precontrast difference image histogram and the fitted model. **(Right)** The three distributions that compose the histogram model.

the segmentation process. The classification is performed using the information from T1 and T2 images only. We also maintain a low base probability of tumor (5%) throughout the brain region. This allows the nonenhancing tumor voxels to still be classified as tumor, provided that they have the same T1 and T2 intensity characteristics as the enhancing tumor voxels.

The contrast enhancement is generally not constrained to only the tumor regions. In most cases, the blood vessels will also be enhanced with the contrast agent. This can cause many misclassifications if left undetected. It is therefore necessary to impose a shape constraint on the tumor prior. To remove the thin, sharp features of the blood vessels, we apply a region competition level-set evolution method (19). This constraint forces the structure within the tumor prior probabilities to be relatively smooth and blobby (Fig 6).

Unlike tumor structures, there is no spatial prior for edema. In general, we have found that edema is mostly found in white matter regions. Therefore, the spatial prior used for edema is a fraction of the white matter prior (20%, obtained experimentally). After the generation of the tumor and edema priors, all the prior probabilities are scaled so that the sum of probabilities at each voxel sum to 1 (Fig 7).

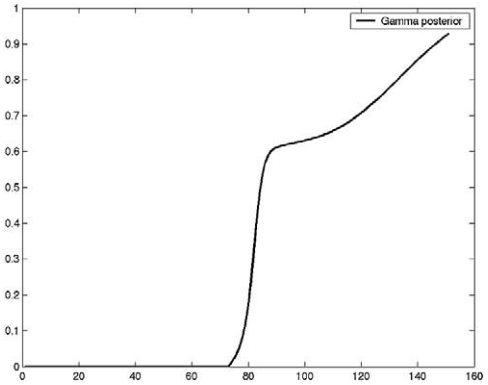

Figure 5. The gamma posterior probability function computed from the T1 postcontrast and precontrast difference image histogram.

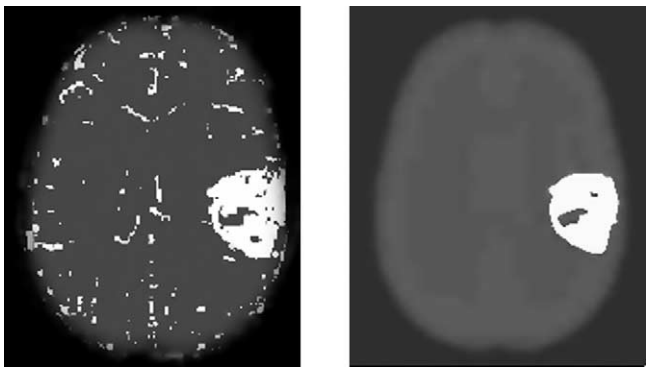

Figure 6. **(Left)** The tumor spatial prior probabilities generated from the difference image. **(Right)** The tumor prior after enforcing the smoothness constraint.

Expectation Maximization Segmentation

The prior probabilities from the atlas and the ones generated for tumor and edema are then passed along with the T1 and T2 images as inputs to the segmentation algorithm. The segmentation algorithm used is the EM segmentation algorithm developed by Van Leemput et al (13,14). The method estimates both the probability density functions of the brain tissue classes and the MR bias field or intensity inhomogeneity. The tissue classes are modeled using a normal or Gaussian distribution. The bias field is assumed to be multiplicative. By applying a logarithmic transform on the image intensities it can be treated as an additive effect. A polynomial function $\Sigma C_k \phi_k(x)$ is used to model the bias field,

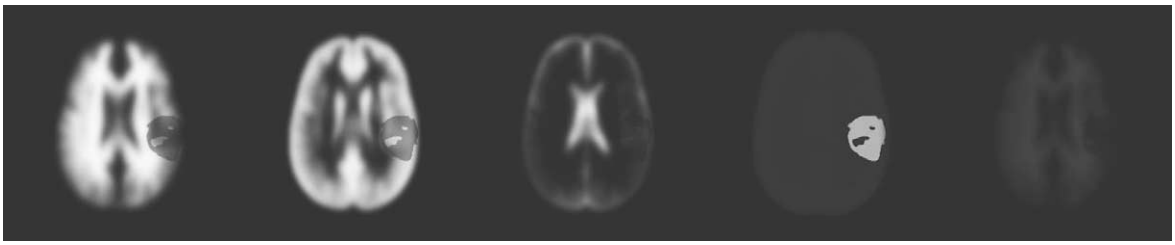

Figure 7. The spatial prior probability maps generated for Tumor020. From left to right: white matter, grey matter, CSF, tumor, and edema.

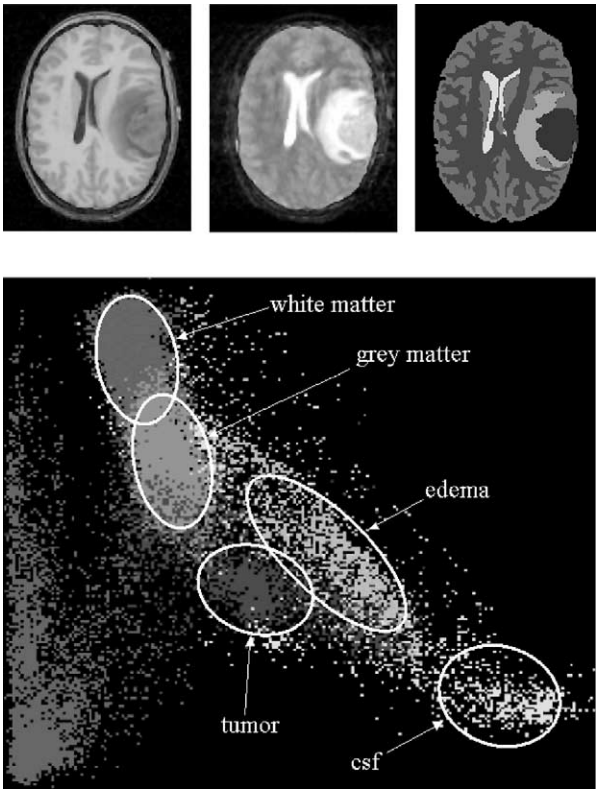

Figure 8. **(Top left)** T1-weighted image. **(Top middle)** T2-weighted image. **(Top right)** Labels from manual segmentation. **(Bottom)** scatterplot of the T1 and T2 intensity features for Tumor020 based on the manual segmentation labels. The horizontal axis represents T2 intensities and the vertical axis represents T1 intensities.

where x indicates a voxel's 3D location, ϕ_k the polynomial basis functions, C_k and the coefficients. The basis functions used are polynomials up to degree 4. The probability that a voxel with intensity features y at location x belongs to class j is then $p(y|\Gamma = j) = G_{\sigma j}(y - \mu_j - \Sigma C_k \phi_k(x))$, with μ_j and σ_j as the mean and covariance for the normal distribution.

The expectation maximization segmentation algorithm interleaves probability distribution estimation for each tissue class, classification, and bias field correction. The probability distributions are initialized using the digital brain atlas. The algorithm then iteratively:

1. classifies the MR data using the current probability distribution and bias field estimates;
2. updates the bias field estimate using the classification;
3. re-estimates the probability distributions from the bias corrected data.

until the probability distributions converge. This method is inspired by the classic EM approach and the seminal work by Wells et al (12). However, adding the bias correction stage causes it to deviate from a pure EM scheme.

The initialization of the distribution parameters for edema is different from the other classes. As stated previously, there is no spatial prior for edema and a fraction of the white matter prior is used. The white matter prior will generally yield a poor estimate of the edema distribution parameters. The edema parameters are estimated after the estimation of the normal tissue parameters. Using prior knowledge of the properties of edema, we initialize the mean for the edema distribution to be between the mean for white matter and CSF. Figure 8 illustrates the intensity distributions for each class. Analysis of the scatter plot would show that this initial mean estimate is reasonably close to the true mean for the edema class.

RESULTS

We applied our automatic segmentation method to five tumor cases. The tool classifies the whole brain into healthy and pathologic regions as shown in Figure 9. The validation of the method is performed with the tumor volumes. For each case, we have two sets of manual segmentations, the second one completed by the same rater more than 3 months after the first. The first set of manual segmentations is cho-

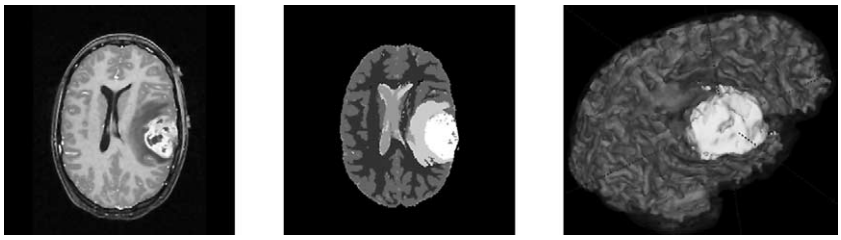

Figure 9. Automatic segmentation result for the Tumor020 data. **(Left)** T1 postcontrast image (for reference). **(Middle)** Labels generated by the automatic method. **(Right)** 3D view of the segmented tumor structure and cortical surface.

sen as a gold standard for the purpose of evaluating the method. As another measure of performance, we also compared the manual segmentation results with the segmentations generated by a semi-automatic segmentation tool that uses level-set evolution (19). The semi-automatic segmentations are generated from the T1 contrast difference image with the user specifying the rough estimate of the tumor location by placing bubbles in the 3D volume. The tool uses this contrast difference image as a foreground/background probability and evolves a smooth surface capturing the tumor boundary. The volumes of the tumor structures for each case are shown in Table 1.

The software used for the evaluation is VALMET (MIDAG, Chapel Hill, NC) (20). VALMET is used to generate two different classes of metrics for comparing two segmentations. The first metric class measures the volume of overlap between the two segmentations. The second metric class computes distances between the surfaces of the segmented structures. Two overlap measures are used. The first compares the volume of intersection with the combined volume, $\frac{(A \cap B)}{(A \cup B)}$. The second compares the volume of intersection with the first volume, $\frac{(A \cap B)}{A}$. If we treat the first segmentation as the gold standard, the second overlap measure ignores the false positives in segmentation B. Both overlap measures have a range of values between 0 (complete disagreement) and 1 (complete agreement). The surface distances used for this evaluation are the average surface distances with inward and outward direction (relative to the first segmented object), the average surface distance (absolute, both inward and outward), and the median surface distance.

The reliability of the manual segmentations is shown in Table 2. For all five cases, there is high degree of overlap and only 1 mm or less average surface distance. Thus, the intra-rater reliability of the manual segmentations is high. Table 3 shows the comparison between the manual segmentation results and the results generated by the semi-automatic level-set evolution tool. The resulting volumes tend to be smaller than manual segmentation volumes, which are reflected in the lower overlap measures and larger surface distance measures. Table 1 also indicates this fact. As shown in Table 4, the performance of the automatic method is consistently below that of the semi-automatic method. However, the automatic segmentation method has the advantage that it has no requirement of user interaction. For the first three of the five cases, the relatively low performance appears to be mainly caused by the number of false positives that the algorithm generates. For visual inspection, we have generated both the 2D and 3D views of the segmented structures generated by the automatic algorithm for the Tu-

Table 1
The Volumes of the Segmented Tumor Structure Generated Using Different Methods, Measured in mm^3

Case	Manual 1	Manual 2	Semi-Automatic	Automatic
Tumor020	35578.6	35114.5	33436.2	43052.3
Tumor022	24290.8	25215.8	22342.6	27305.6
Tumor025	24742.4	27802	26093.6	45800.4
Tumor031	72503	76842	65881	67907
Tumor032	56262.3	56807.4	47984.9	41925.3

Table 2
A List of Metrics Comparing the Two Segmentations From the same Human Rater, Which Shows the Intra-Rater Variability for each Case

Case	Overlap 1	Overlap 2	Average Distance In	Average Distance Out	Average Distance	Median Distance
Tumor020	0.89	0.936	0.32	1.17	0.53	0
Tumor022	0.828	0.923	0.34	1.21	0.73	0.89
Tumor025	0.812	0.952	0.21	1.31	0.73	0.89
Tumor031	0.827	0.932	0.64	1.66	1.16	1.00
Tumor032	0.881	0.941	0.26	1.39	0.54	0

NOTE. The second set of segmentations is done following the first set after a period of more than 3 months. All distances are in millimeters.

mor020 data (Fig 9). On average, the segmentation process for one dataset takes 1 hour and 40 minutes on a 2GHz Intel Xeon machine (Intel, Santa Clara, CA).

CONCLUSION

We have developed a model-based segmentation method for segmenting head MR image datasets with tumors and infiltrating edema. This is achieved by extending the spatial prior of a statistical normal human brain atlas with individual information derived from the patient's dataset. Thus, we combine the statistical geometric prior with image-specific information for both geometry of newly appearing objects and probability density functions for healthy tissue and pathology. Applications to five tumor patients with variable tumor appearance showed that the procedure could handle large variation of tumor size, interior texture, and locality. The automatic procedure was compared with tumor segmentation by manual outlining and by using semi-automated level-set evolution tool. However, the significant benefits are increased efficiency and the segmentation of the whole brain structure including health tissue, tumor, and edema. Embedding tumor and edema into the proper 3D anatomic context is crucial for planning, intervention, and monitoring.

Table 3
A List of Metrics Comparing the First Set of Manual Segmentations and the Results Generated Using the Semi-Automatic Level-Set Evolution Method

Case	Overlap 1	Overlap 2	Average Distance In	Average Distance Out	Average Distance	Median Distance
Tumor020	0.873	0.904	0.47	1.13	0.60	0
Tumor022	0.85	0.882	0.34	1.01	0.47	0
Tumor025	0.763	0.889	0.57	1.42	0.89	0.89
Tumor031	0.813	0.856	1.13	1.63	1.27	1.00
Tumor032	0.789	0.817	1.39	1.40	1.39	0.86

NOTE. All distances are in millimeters.

Table 4
A List of Metrics Comparing the First Set of Manual Segmentations and the Results of the Automatic Segmentation Method

Case	Overlap 1	Overlap 2	Average Distance In	Average Distance Out	Average Distance	Median Distance
Tumor020	0.71	0.918	1.92	2.54	2.25	1.77
Tumor022	0.57	0.771	1.69	3.29	2.59	2.01
Tumor025	0.49	0.937	1.28	4.94	4.21	3.24
Tumor031	0.586	0.716	3.79	3.25	3.57	2.83
Tumor032	0.578	0.639	3.59	3.52	3.56	3.0

NOTE. All distances are in millimeters.

The automatic method does not perform as well as the semi-automatic method. However, it generates a fully reproducible whole brain segmentation with embedded pathology and requires a lower degree of user supervision. The full brain segmentation provides anatomic context, which may help in therapy planning and detecting deviation from normal. The clinical consequences of the lower level of agreement with the manual raters cannot be fully explored because of the limited number of cases. The results have been used in the analysis of vessel attributes in tumor volumes (21,22). Compared with the results obtained with manual tumor segmentations, we observed no significant difference.

The lower agreement with the manual rater can be explained in terms of the underlying model. This method does voxel-by-voxel classification as opposed to a human rater who uses high-level human vision coupled with specialized domain knowledge. Discrimination by voxel intensities and the simplified geometric model for tumor shape cannot cope with tumors that have complex appearance and ambiguous boundaries. Furthermore, the lack of a true gold standard for healthy tissue and tumor is an inherent problem for validation.

In our future work, we will study the issue of deformation of normal anatomy in the presence of space-occupying tumors. Within the range of tumors studied to date, the soft boundaries of the statistical atlas (Fig 2) could handle spatial deformation. However, we will develop a scheme for high dimensional warping of multichannel probability data to get a better match between atlas and deformed patient images.

The VALMET (MIDAG, Chapel Hill, NC) validation software and the SNAP (MIDAG) level-set evolution segmentation software are available for free download through the MIDAG home page http://midag.cs.unc.edu.

ACKNOWLEDGMENTS

We acknowledge K.U. Leuven for providing the MIRIT image registration software.

REFERENCES

1. Just M, Thelen M. Tissue characterization with T1, T2, and proton density values: results in 160 patients with brain tumors. Radiology 1988; 2:779–785.
2. Gerig G, Martin J, Kikinis R, Kubler O, Shenton M, Jolesz F. Automating segmentation of dual-echo MR head data. In: Colchester A, Hawkes D, eds. Proceedings of Information Processing in Medical Imaging 1991 Springer Lecture Notes in Computer Science 511. Berlin: Springer; 1991, 175–185.
3. Velthuizen R, Clarke L, Phuphianich S, et al. Unsupervised measurement of brain tumor volume on MR images. J Magn Reson Imaging 1995; 4:594–605.
4. Vinitski S, Gonzales C, Mohamed F, Iwanaga T, Knobler R, Khalili K, Mack J. Improved intracranial lesion characterization by tissue segmentation based on a 3D feature map. Magn Reson Med 1997; 5:457–469.
5. Kamber M, Shingal R, Collins D, Francis D, Evans A. Model-based, 3-D segmentation of multiple sclerosis lesions in magnetic resonance brain images. IEEE Trans Med Imaging 1995; 6:442–453.
6. Zijdenbos A, Forghani R, Evans A. Automatic quantification of MS lesions in 3D MRI brain data sets: validation of INSECT. In: Wells W, Colchester A, Delp S, eds. Proceedings of the Medical Image Computing and Computer-Assisted Intervention, Cambridge, MA 1998. Springer Lecture Notes in Computer Science series 1496. Berlin: Springer; 1998, 439–448.
7. Vehkomaki T, Gerig G, Szekely G. A user-guided tool for efficient segmentation of medical image data. In: Troccas J, Grimson W, Mosges R, eds. Proceedings of Computer Vision, Virtual Reality, and Robotics in Medicine—Medical Robotics and Computer-Assisted Surgery 1997. Lecture Notes in Computer Science 1205. Berlin: Springer; 1997, 685–694.
8. Gibbs P, Buckley D, Blackband S, Horsman A. Tumour volume determination from MR images by morphological segmentation. Phys Med Biol 1996; 13:2437–2446.
9. Kjaer L, Ring P, Thomson C, Henriksen O. Texture analysis in quantitative MR imaging: tissue characterization of normal brain and intracranial tumors at 1.5 T. Acta Radiol 1995; 36:127–135.
10. Warfield S, Dengler J, Zaers J, et al. Automatic identification of gray matter structures from MRI to improve the segmentation of white matter lesions. J Image Guid Surg 1995; 1:326–338.
11. Warfield S, Kaus M, Jolesz F, Kikinis R. Adaptive template moderated spatially varying statistical classification. In: Wells W, Colchester A, Delp S, eds. Proceedings of the Medical Image Computing and Computer-Assisted Intervention, Cambridge, MA 1998. Springer Lecture Notes in Computer Science 1496. Berlin: Springer; 1998, 431–438.
12. Wells W, Kikinis R, Grimson W, Jolesz F. Adaptive segmentation of MRI data. IEEE Trans Med Imaging 1996; 18:429–442.
13. Van Leemput K, Maes F, Vandermeulen D, Suetens P. Automated model based tissue classification of MR images of the brain. IEEE Trans Med Imaging 1999; 18:897–908.
14. Van Leemput K, Maes F, Vandermeulen D, Suetens P. Automated model based bias field correction of MR images of the brain. IEEE Trans Med Imaging 1999; 18:885–896.
15. Van Leemput K, Maes F, Vandermeulen D, Colchester A, Suetens P. Automated segmentation of multiple sclerosis lesions by model outlier detection. IEEE Trans Med Imaging 2001; 20:677–688.
16. Moon N, Bullitt E, Van Leemput K, Gerig, G. Automatic brain and tumor segmentation. In: Dohi T, Kikinis R, eds. Proceedings of the Medical Image Computing and Computer-Assisted Intervention, Tokyo: Springer Lecture Notes I in Computer Science 2488; 2002; 372–379.
17. Evans A, Collins D, Mills S, Brown E, Kelly R, Peters T. 3D statistical neuroanatomical models from 305 MRI volumes. In: Proc. IEEE Nuclear Science Symposium and Medical Imaging Conference; 1993; 1813–1817.
18. Maes F, Collignon A, Vandermeulen D, Marchal G, Suetens P. Multimodality image registration by maximization of mutual information. IEEE Trans Med Imaging 1997; 16:187–198.
19. Ho S, Bullitt E, Gerig G. Level set evolution with region competition: automatic 3-D segmentation of brain tumors. In: Katsuri R, Laurendeau D, Suen C, eds. Proc. 16th International Conference on Pattern Recognition; 2002; 532–535.
20. Gerig G, Jomier M, Chakos M. VALMET: a new validation tool for assessing and improving 3D object segmentation. In: Niessen W, Viergever M, eds. Proceedings of the Medical Image Computing and Computer-Assisted Intervention. Springer Lecture Notes in Computer Science 2208; 2001; 516–523.
21. Bullitt E, Gerig G, Pizer SM, Lin W, Aylward SR. Measuring tortuosity of the intracerebral vasculature from MRA images. IEEE Trans Med Imaging TMI 2003; 22:1163–1171.
22. Bullitt E, Gerig G, Aylward S, Joshi S, Smith K, Ewend M, Lin W. Vascular attributes and malignant brain tumors. In: Ellis R, Peters T, eds. Proceedings of the Medical Image Computing and Computer-Assisted Intervention, Tokyo: 2003 Springer Lecture Notes I in Computer Science; in press.